v2.2

Femtoscopy in $p+p$ collisions at RHIC

PAs: Zbigniew Chajęcki, Mike Lisa for the STAR Collaboration

(Dated: December 16, 2009)

The STAR Collaboration at RHIC has measured two-pion correlation functions from p+p collisions at 200 GeV. Spatial scales are extracted via a femtoscopic analysis of the correlations, though this analysis is complicated by the presence of strong non-femtoscopic effects. Our results are put into the context of the world dataset of femtoscopy in hadron-hadron collisions. We present the first direct comparison of femtoscopy in p+p and heavy ion collisions, under identical analysis and detector conditions.

I. INTRODUCTION AND MOTIVATION

Studies of ultrarelativistic heavy ion collisions aim to explore the equation of state of strongly interacting matter. The highly dynamic nature of the collisions, however, does not allow a purely statistical study of static matter as one might perform in condensed matter physics, but rather requires a detailed understanding of the dynamics itself. If a bulk, self-interacting system is formed (something that should not be assumed *a priori*), the equation of state then plays the dynamic role of generating pressure gradients that drive the collective expansion of the system. Copious evidence [1–4] indicates that a self-interacting system is, in fact, generated in these collisions. The dynamics of the bulk medium is reflected in the transverse momentum (p_T) distribution [5, 6] and momentum-space anisotropy (e.g. "elliptic flow") [7, 8] of identified particles in the soft sector– i.e. at low p_T. These observables are well-described in a hydrodynamic scenario, in which a nearly perfect (i.e. very low viscocity) fluid expands explosively under the action of pressure gradients induced by the collision [9].

Two-particle femtoscopy [10] (often called "HBT" analysis) measures the space-time substructure of the emitting source at "freeze-out," the point at which particles decouple from the system [e.g. 11]. Femtoscopic measuresments play a special role in understanding bulk dynamics in heavy ion collisions, for several reasons. Firstly, collective flow generates characteristic space-momentum patterns at freeze-out that are revealed [11] in the momentum-dependence of pion "HBT radii" (discussed below), the mass dependence of homogeneity lengths [12], and non-identical particle correlations [13]. Secondly, while a simultaneous description of particle-identified p_T distributions, elliptic flow and femtoscopic measurements is easily achieved in flow-dominated toy models [e.g. 6], achieving the same level of agreement in a realistic transport calculation is considerably more challenging. In particular, addressing this "HBT puzzle" [14] has led to a deeper understanding of the freezeout hypersurface, collectivity in the initial stage, and the equation of state. Femtoscopic signals of long dynamical timescales expected for a system undergoing a first-order phase transition [15, 16], have not been observed [11], providing early evidence that the system at RHIC evolves from QGP to hadron gas via a crossover [17]. This sensitive and unique connection to important underlying physics has motivated a huge systematics of femtoscopic measurements in heavy ion collisions over the past quarter century [11].

HBT correlations from hadron (e.g. $p+p$) and lepton (e.g. $e^+ + e^-$) collisions have been extensively studied in the high energy physics community, as well [18–20], although the theoretical interpretation of the results is less clear and well developed. Until now, it has been impossible to quantitatively compare femtoscopic results from hadron-hadron collisions to those from heavy ion collisions, due to divergent and often undocumented analysis techniques, detector acceptances and fitting functions historically used in the high energy community [20].

In this paper, we exploit the unique opportunity offered by the STAR/RHIC experiment, to make the first direct comparison and quantitative connection between femtoscopy in proton-proton and heavy ion collisions. Systematic complications in comparing these collisions are greatly reduced by using identical detector and reconstruction system, collision energies, and analysis techniques (e.g. event mixing [21], see below). We observe and discuss the importance of non-femtoscopic correlations in the analysis of small systems, and put our femtoscopic results for $p+p$ collisions into the context both of heavy ion collisions and (as much as possible) into the context of previous high-energy measurements on hadron-hadron and $e-e$ collisions. We hope that our results may eventually lead to a deeper understanding of the physics behind the space-momentum correlations in these collisions, in the same way that comparison of $p+p$ and heavy ion collision results in the high-p_T sector is crucial for understanding the physics of partonic energy loss [1–4, 22]. Our direct comparison also serves as a model and baseline for similar comparisons soon to be possible at higher energies at the Large Hadron Collider.

The paper is organized as follows. In Section II, we discuss the construction of the correlation function and the forms used to parameterize it. Section III discusses details of the analysis, and the results are presented in Section IV. In Section V, we put these results in the context of previous measurements in $Au+Au$ and elementary particle collisions. We discuss the similarity between the systematics of HBT radii in heavy ion and particle collisions in Section VI and summarize in Section VII.

II. TWO-PARTICLE CORRELATION FUNCTION

The two-particle correlation function is generally defined as the ratio of the probability of the simultaneous meaurement of measuring two particles with momenta p_1 and p_2, to the product of single particle probabilities,

$$C(\vec{p}_1,\vec{p}_2) \equiv \frac{P(\vec{p}_1,\vec{p}_2)}{P(\vec{p}_1)P(\vec{p}_2)}. \tag{1}$$

In practice, one usually studies the quantity

$$C_{\vec{P}}(\vec{q}) = \frac{A_{\vec{P}}(\vec{q})}{B_{\vec{P}}(\vec{q})}, \tag{2}$$

where $\vec{q} \equiv \vec{p}_1 - \vec{p}_2$. $A(\vec{q})$ is the distribution of the pairs from the same event, and $B(\vec{q})$ is the reference (or "background") distribution. B contains all single-particle effects, including detector acceptance and efficiency, and is usually calculated with an event-mixing technique [11, 21]. The explicit label $\vec{P}$ ($\equiv \vec{p}_1 + \vec{p}_2$) emphasizes that separate correlation functions are constructed and fitted (see below) as a function of $\vec{q}$, for different selections of the total momentum $\vec{P}$; following convention, we drop the explicit subscript below. Sometimes the measured ratio is normalized to unity at large values of $|\vec{q}|$; we include the normalization in the fit.

In older or statistics-challenged experiments, the correlation function is sometimes constructed in the one-dimensional quantity $Q_{inv} \equiv \sqrt{(\vec{p}_1 - \vec{p}_2)^2 - (E_1 - E_2)^2}$ or two-dimensional variants (see below). More commonly in recent experiments, it is constructed in three dimensions in the so-called the Pratt-Bertsch "out-side-long" coordinate system [23, 24]. In this system, the "out" direction is that of the pair transverse momentum, the "long" direction is parallel to the beam, and the "side" direction is orthogonal to these two. We will use the subscripts "o," "l" and "s" to indicate quantities in these directions.

It has been suggested [25–27] to construct the three-dimensional correlation function using spherical coordinates

$$q_o = |\vec{q}|\sin\theta\cos\phi, \qquad q_s = |\vec{q}|\sin\theta\sin\phi, \qquad q_l = |\vec{q}|\cos\theta. \tag{3}$$

This aids in making a direct comparison to the spatial separation distribution through imaging techniques and provides an efficient way to visualize the full three-dimensional structure of $C(\vec{q})$. The more traditional "Cartesian projections" in the "o," "s," and "l" directions integrate over most of the three-dimensional structure, especially at large relative momentum [11, 27].

Below, we will present data in the form of the spherical harmonic decomposition coefficients, which depend explicitly on $|\vec{q}|$ as

$$A_{l,m}(|\vec{q}|) \equiv \frac{1}{\sqrt{4\pi}} \int d\phi d(\cos\theta) C(|\vec{q}|,\theta,\phi)\, Y_{l,m}(\theta,\phi). \tag{4}$$

The coefficient $A_{00}(|\vec{q}|)$ represents the overall angle-integrated strength of the correlation. $A_{20}(|\vec{q}|)$ and $A_{22}(|\vec{q}|)$ are the quadrupole moments of C at a particular value of $|\vec{q}|$. In particular, A_{22} quantifies the second-order oscillation about the "long" direction; in the simplest HBT analysis, this term reflects non-identical values of the R_{out} and R_{side} HBT radii (c.f. below). Coefficients with odd l represent a dipole moment of the correlation function and correspond to a "shift" in the average position of the first particle in a pair, relative to the second [25–27]. In the present case of identical particles, the labels "first" and "second" become meaningless, and odd-l terms vanish by symmetry. Likewise, for the present case, odd-m terms, and all imaginary components vanish as well. See Appendix B of [27] for a full discussion of symmetries.

In heavy ion collisions, it is usually assumed that all of the correlations between identical pions at low relative momentum are due to femtoscopic effects, i.e. quantum statistics and final-state interactions [11]. At large $|\vec{q}|$, femtoscopic effects vanish [e.g. 11]. Thus, in the absence of other correlations, $C(\vec{q})$ must approach a constant value independent of the magnitude and direction of $\vec{q}$; equivalently, $A_{l,m}(|\vec{q}|)$ must vanish at large $|\vec{q}|$ for $l \neq 0$.

However, in elementary particle collisions additional structure at large relative momentum ($|\vec{q}| \gtrsim 400$ MeV/c) has been observed [e.g. 20, 28–32]. Usually this structure is parameterized in terms of a function $\Omega(\vec{q})$ that contributes in addition to the femtoscopic component $C_F(\vec{q})$. Explicitly including the normalization parameter $\mathcal{N}$, then, we will fit our measured correlation functions with the form

$$C(\vec{q}) = \mathcal{N} \cdot C_F(\vec{q}) \cdot \Omega(\vec{q}). \tag{5}$$

Below, we discuss separately various parameterizations of the femtoscopic and non-femtoscopic components, which we use in order to connect with previous measurements. A historical discussion of these forms may be found in [20].

A. Femtoscopic correlations

Femtoscopic correlations between identical pions are dominated by Bose-Einstein symmetrization and Coulomb final state effects in the two-pion wavefunction [11].

In all parameterizations, the overall strength of the femtoscopic correlation is characterized by a parameter λ [11]. Historically misnamed the "chaoticity" parameter, it generally accounts for particle identification efficiency, long-lived decays, and long-range tails in the separation distribution.

In the simplest case, the Bose-Einstein correlations are often parameterized by a Gaussian,

$$C_F(Q_{inv}) = 1 + \lambda e^{-Q_{inv}^2 R_{inv}^2}, \tag{6}$$

where R_{inv} is a one dimensional "HBT radius."

Another historical parameterization uses the energy difference $q_0 = E_1 - E_2$ and the magnitude of the vector momentum difference in the laboratory frame:

$$C_F(q,q_0) = 1 + \lambda e^{-|\vec{q}|^2 R_G^2 - q_0^2 \tau^2}. \tag{7}$$

Here, R_G and τ are parameters characterizing the source size and lifetime.

Kopylov and Podgoretskii [33] introduced an alternative parameterization

$$C_F(q_T,q_0) = 1+\lambda\left[\frac{2J_1(q_TR_B)}{q_TR_B}\right]^2\left(1+q_0^2\tau^2\right)^{-1}, \quad (8)$$

where q_T is the component of $\vec{q}$ orthogonal to $\vec{P}$, $q_0 = E_1 - E_2$, R_B and τ are the size and decay constants of a spherical emitting source, and J_1 is the first order Bessel function.

Simple numerical studies show that R_G from Eq. 7 is approximately half as large as R_B obtained from Eq. 8 [20, 34, 35].

With sufficient statistics, a three-dimensional correlation function may be measured. We calculate the relative momentum in the longitudinally co-moving system (LCMS), in which the total longitudinal momentum of the pair, $p_{l,1}+p_{l,2}$, vanishes. For heavy ion and hadron-hadron collisions, this "longitudinal" direction $\hat{l}$ is taken to be the beam axis [11]; for $e^+ + e^-$ collisions, the thrust axis is used.

For a Gaussian emission source, femtoscopic correlations due only to Bose-Einstein symmetrization are given by [e.g. 11]

$$C_F(q_o,q_s,q_l) = 1+\lambda e^{-q_o^2R_o^2-q_s^2R_s^2-q_l^2R_l^2}, \quad (9)$$

where R_o, R_s and R_l are the spatial scales of the source.

While older papers sometimes ignored the Coulomb final-state interaction between the charged pions [20], it is usually included by using the Bowler-Sinyukov [36, 37] functional form

$$C_F(Q_{inv}) = (1-\lambda)+\lambda K_{\mathrm{coul}}(Q_{inv})\left(1+e^{-Q_{inv}^2R_{inv}^2}\right), \quad (10)$$

and in 3D,

$$\begin{aligned} C_F(q_o,q_s,q_l) \;=\; & (1-\lambda)+\lambda K_{\mathrm{coul}}(Q_{inv}) \\ & \times\left(1+e^{-q_o^2R_o^2-q_s^2R_s^2-q_l^2R_l^2}\right). \quad (11)\end{aligned}$$

Here, K_{coul} is the squared Coulomb wavefunction integrated over the source.

B. Non-femtoscopic correlations

In the absence of non-femtoscopic effects, one of the forms for $C_F(\vec{q})$ from Section II A is fitted to the measured correlation function; i.e. $\Omega = 1$ in Equation 5. Such a "standard fit" works well in the high-multiplicity environment of heavy ion collisions [11]. In hadron-hadron or $e+e$ collisions, however, it does not describe the measured correlation function well, especially as $|q|$ increases. Most authors attribute the non-femtoscopic structure to momentum conservation effects in these small systems. While this large-$|q|$ behavior is sometimes simply ignored, it is usually included in the fit either through ad-hoc [29] or physically-motivated [27] terms.

In this paper, we will use three selected parameterizations of the non-femtoscopic correlations and study their effects on the femtoscopic parameters obtained from the fit to experimental correlation functions. The first formula assumes that the non-femtoscopic contribution can be parameterized by a first-order polynomial in q-components (used e.g. in [38–42]). Respectively, the one- and three-dimensional forms used in the literature are

$$\Omega(q) = 1+\delta q \quad (12)$$

and

$$\Omega(\vec{q}) = \Omega(q_o,q_s,q_l) = 1+\delta_o q_o+\delta_s q_s+\delta_l q_l. \quad (13)$$

For simplicity, we will use the name "$\delta-q$ fit" when the above formula was used in the fitting procedure.

Another form [43] assumes that non-femtoscopic correlations contribute $|\vec{q}|$-independent values to the $l=2$ moments in Equation 4. In terms of the fitting parameters ζ and β,

$$\begin{aligned}\Omega(|\vec{q}|,\cos\theta,\phi) = \Omega(\cos\theta,\phi) = \\ 1+2\sqrt{\pi}(\beta Y_{2,0}+2\zeta Y_{2,2}) = \\ 1+\beta\sqrt{\frac{5}{4}}(3\cos^2\theta-1)+\zeta\sqrt{\frac{15}{2}}\sin^2\theta\cos 2\phi. \quad (14)\end{aligned}$$

For simplicity, fits using this form for the non-femtoscopic effects will be referred to as "$\zeta-\beta$ fits."

These two forms (as well as others that can be found in literature [20]) are purely empirical, motivated essentially by the shape of the observed correlation function itself. While most authors attribute these effects primarily to momentum conservation in these low-multiplicity systems, the parameters and functional forms themselves cannot be directly connected to this or any physical mechanism. One may identify two dangers of using an ad-hoc form to quantify non-femtoscopic contributions to $C(\vec{q})$. Firstly, while they describe (by construction) the correlation function well at large $|\vec{q}|$, for which femtoscopic contributions vanish, there is no way to constrain their behaviour at low $|\vec{q}|$ where both femtoscopic and (presumably) non-femtoscopic correlations exist. Even simple effects like momentum conservation give rise to non-femtoscopic correlations that vary non-trivially even at low $|\vec{q}|$. Misrepresenting the non-femtoscopic contribution in $\Omega(\vec{q})$ can therefore distort the femtoscopic radius parameters in $C_F(\vec{q})$. Secondly, there is no way to estimate whether the best-fit parameter values in an ad-hoc functional form are "reasonable," given the physics they are intended to parameterize.

If the non-femtoscopic correlations are in fact dominated by energy and momentum conservation, as is usually supposed, one may derive an analytic functional form for Ω. In particular, the multiparticle phasespace constraints for a system of N particles project onto the two-particle space as [27]

$$\begin{aligned}\Omega(p_1,p_2) = & 1-M_1\cdot\overline{\{\vec{p}_{1,T}\cdot\vec{p}_{2,T}\}}-M_2\cdot\overline{\{p_{1,z}\cdot p_{2,z}\}} \quad (15) \\ & -M_3\cdot\overline{\{E_1\cdot E_2\}}+M_4\cdot\overline{\{E_1+E_2\}}-\frac{M_4^2}{M_3},\end{aligned}$$

where

$$M_1 \equiv \frac{2}{N\langle p_T^2\rangle}, \qquad M_2 \equiv \frac{1}{N\langle p_z^2\rangle}$$
$$M_3 \equiv \frac{1}{N\left(\langle E^2\rangle - \langle E\rangle^2\right)}, \quad M_4 \equiv \frac{\langle E\rangle}{N\left(\langle E^2\rangle - \langle E\rangle^2\right)}. \qquad (16)$$

The notation $\overline{\{X\}}$ in Equation 15 is used to indicate that X is a two-particle quantity which depends on p_1 and p_2 (or $\vec{q}$, etc). In practice, this means generating histograms in addition to $A(\vec{q})$ and $B(\vec{q})$ (c.f. Equation 2) as one loops over pairs in the data analysis. For example

$$\overline{\{\vec{p}_{1,T}\cdot\vec{p}_{2,T}\}}(\vec{q}) = \frac{\sum_{i,j}\vec{p}_{i,T}\cdot\vec{p}_{j,T}}{B(\vec{q})}, \qquad (17)$$

where the sum in the numerator runs over all pairs in all events.

In Equation 15, the four fit parameters M_i are directly related to five physical quantities, (N - the number of particles, $\langle p_T^2\rangle$, $\langle p_z^2\rangle$, $\langle E^2\rangle$, $\langle E\rangle$) through Eq. 16. Assuming that

$$\langle E^2\rangle \approx \langle p_T^2\rangle + \langle p_z^2\rangle + m_*^2, \qquad (18)$$

where m_* is the mass of a typical particle in the system (for our pion-dominated system, $m_* \approx m_\pi$), then one may solve for the physical parameters. For example,

$$N \approx \frac{M_1^{-1} + M_2^{-1} - M_3^{-1}}{\left(\frac{M_4}{M_3}\right)^2 - m_*^2}. \qquad (19)$$

Since we cannot know exactly the values of $\langle E^2\rangle$ etc, that characterize the underlying distribution in these collisions, we treat the M_i as free parameters in our fits, and then consider whether their values are mutually compatible and physical. For a more complete discussion, see [27, 44].

In [27], the correlations leading to Equation 15 were called "EMCICs" (short for Energy and Momentum Conservation-Induced Correlations); we will refer to fits using this function with this acronym, in our figures.

C. Parameter counting

As mentioned, we will be employing a number of different fitting functions, each of which contains several parameters. It is appropriate at this point to breifly take stock.

In essentially all modern HBT analyses, on the order of 5-6 parameters quantify the femtoscopic correlations. For the common Gaussian fit (equation 11), one has three "HBT radii," the chaoticity parameter, and the normalization $\mathcal{N}$. Recent "imaging" fits approximate the two-particle emission zone as a sum of spline functions, the weights of which are the parameters; the number of splines (hence weights) used is ~ 5. Other fits (double Gaussian, exponential-plus-Gaussian) contain a similar number of femtoscopic parameters. In all cases, a distinct set of parameters is extracted for each selection of $\vec{P}$ (c.f. equation 2 and surrounding discussion).

Accounting for the non-femtoscopic correlations inevitably increases the total number of fit parameters. The "$\zeta-\beta$" functional form (eq. 14) involves two parameters, the "$\delta-q$" form (eq. 13) three, and the EMCIC form (eq. 15) four. However, it is important to keep in mind that using the $\zeta-\beta$ ($\delta-q$) form means 2 (3) additional parameters *for each selection* of $\vec{P}$ when forming the correlation functions. On the other hand, the four EMCICs parameters cannot depend on $\vec{P}$. Therefore, when fitting $C_{\vec{P}}(\vec{q})$ for four selections of $\vec{P}$, use of the $\zeta-\beta$, $\delta-q$ and EMCIC forms increases the total number of parameters by 8, 12 and 4, respectively.

III. ANALYSIS DETAILS

As mentioned in Section I, there is significant advantage in analyzing $p+p$ collisions in the same way that heavy ion collisions are analyzed. Therefore, the results discussed in this paper are produced with the same techniques and acceptance cuts as have been used for previous pion femtoscopy studies by STAR [45–48]. Here we discuss some of the main points; full systematic studies of cuts and techniques can be found in [47].

The primary sub-detector used in this analysis to reconstruct particles is the Time Projection Chamber (TPC) [49]. Pions could be identified up to a momentum of 800 MeV/c by correlating their the momentum and specific ionization loss (dE/dx) in the TPC gas. A particle was considered to be a pion if its dE/dx value for a given momentum was within two sigma of the Bethe-Bloch expectation for a pion, and more than two sigma from the expectations for electrons, kaons and protons. The small contamination due to electrons and kaons impacts mostly the value of λ obtained from the fit while it was only a 1% effect of the femtoscopic radii. The lower momentum cut of 120 MeV/c is imposed by the TPC acceptance and the magnetic field. Only tracks at midrapidity ($|y| < 0.5$) were included in the femtoscopic analysis. Events were selected for analysis if the primary collision vertex was within 30 cm of the center of the TPC. The further requirement that events include at least two like-sign pions increases the average charged particle multiplicity with pseudorapidity $|\eta| < 0.5$ from 3.0 (without the requirement) to 4.25. Since particle *pairs* enter into the correlation function, the effective average multiplicity is higher; in particular, the pair-weighted charged-particle multiplicity at midrapidity is about 6.0. After event cuts, about 5 million minimum bias events from $p+p$ collisions at $\sqrt{s}$=200 GeV were used.

Two-track effects, such as splitting (one particle reconstructed as two tracks) and merging (two particles reconstructed as one track) were treated identically as has been done in STAR analyses of Au+Au collisions [47]. Both effects can affect the shape of $C(\vec{q})$ at very low $|\vec{q}| \lesssim 20$ MeV/c, regardless of the colliding system. However, their effect on the extracted sizes in $p+p$ collisions turns out to be smaller than statistical errors, due to the fact that small (~ 1 fm) sources lead to large (~ 200 MeV/c) femtoscopic structures in the correlation function.

The analysis presented in this paper was done for four bins in average transverse momentum k_T ($\equiv \frac{1}{2}|(\vec{p}_{T,1}+\vec{p}_{T,2})|$): 150-250, 250-350, 350-450 and 450-600 MeV/c. The systematic errors due to the fit range, particle mis-identification, two-track effects and the Coulomb radius (used to calculate $K_{\rm coul}$ in Eqs. 10 and 11) are estimated to be about 10%, similar to previous studies [47].

IV. RESULTS

In this section, we present the correlation functions and fits to them, using the various functional forms discussed in Section II. The m_T and multiplicity dependence of femtoscopic radii from these fits are compared here, and put into the broader context of data from heavy ion and particle collisions in the next section.

Figure 1 shows the two-pion correlation function for minimum-bias $p+p$ collisions for $0.35 < k_T < 0.45$ GeV/c. The three-dimensional data is represented with the traditional one-dimensional Cartesian projections [11]. For the projection on q_o, integration in q_s and q_l was done over the range $[0.00, 0.12]$ GeV/c. As discussed in Section II and in more detail in [27], the full structure of the correlation function is best seen in the spherical harmonic decomposition, shown in Figures 2-5.

In what follows, we discuss systematics of fits to the correlation function, with particular attention to the femtoscopic parameters. It is important to keep in mind that the fits are performed on the full three-dimensional correlation function $C(\vec{q})$. The choice to plot the data and fits as spherical harmonic coefficients A_{lm} or as Cartesian projections along the "out," "side" and "long" directions is based on the determination to present results in the traditional format (projections) or in a representation more sensitive to the three-dimensional structure of the data [27]. In particular, the data and fits shown in Figure 1, for k_T=0.35-0.45 GeV/c, are the same as those shown in Figure 4.

A. Transverse mass dependence of 3D femtoscopic radii

Femtoscopic scales from three-dimensional correlation functions are usually extracted by fitting to the functional form given in Equation 11. In order to make connection to previous measurements, we employ the same form and vary the treatment of non-femtoscopic effects as discussed in Section II B. The fits are shown as curves in Figures 1-5; the slightly fluctuating structure observable in the sensitive spherical harmonic representation in Figures 2-5 results from finite-binning effects in plotting [50].

Green curves in Figures 1-5 represent the "standard fit," in which non-femtoscopic correlations are neglected altogether ($\Omega = 1$). Black dotted and golden dashed curves, respectively, indicate "$\delta - q$" (Equation 13) and "$\zeta - \beta$" (Equation 14) forms. Red curves represent fits in which the non-femtoscopic contributions follow the EMCIC (Equation 15) form. None of the functional forms perfectly fits the experimental correlation function, though the non-femtoscopic structure is semi-quantitatively reproduced by the ad-hoc $\delta - q$ and $\zeta - \beta$ fits (by construction) and the EMCIC fit (non-trivially). Rather

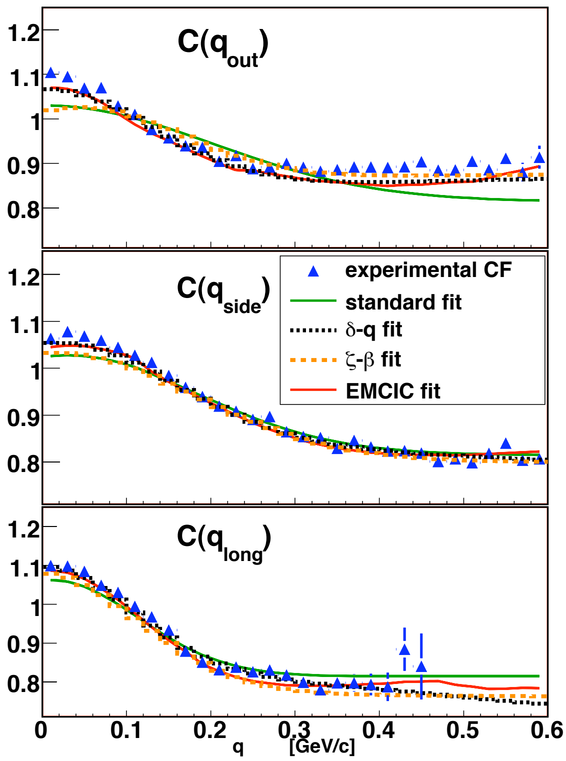

FIG. 1: (Color online) Cartesian projections of the 3D correlation function from $p+p$ collisions at $\sqrt{s}$=200 GeV for $k_T = [0.35, 0.45]$ GeV/c (blue triangles). Femtoscopic effects are parameterized with the form in Eq. 11; different curves represent various parameterizations of non-femtoscopic correlations used in the fit and described in detail in Sec. II B.

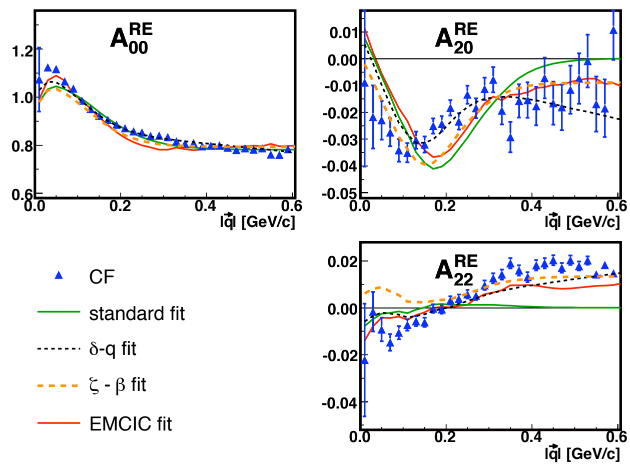

FIG. 2: (Color online) The first three non-vanishing moments of the spherical harmonic decomposition of the correlation function from $p+p$ collisions at $\sqrt{s}$=200 GeV, for $k_T = [0.15, 0.25]$ GeV/c. Femtoscopic effects are parameterized with the form in Eq. 11; different curves represent various parameterizations of non-femtoscopic correlations used in the fit and described in detail in Sec. II B.

k_T [GeV/c]	R_o [fm]	R_s [fm]	R_l [fm]	λ
$[0.15, 0.25]$	0.84 ± 0.02	0.89 ± 0.01	1.53 ± 0.02	0.422 ± 0.004
$[0.25, 0.35]$	0.81 ± 0.02	0.88 ± 0.01	1.45 ± 0.02	0.422 ± 0.005
$[0.35, 0.45]$	0.71 ± 0.02	0.82 ± 0.02	1.31 ± 0.02	0.433 ± 0.007
$[0.45, 0.60]$	0.68 ± 0.02	0.68 ± 0.01	1.05 ± 0.02	0.515 ± 0.009

TABLE I: Fit results from a fit to data from $p+p$ collisions at $\sqrt{s}$= 200 GeV using Eq. 11 to parameterize the femtoscopic correlations ("standard fit").

k_T [GeV/c]	R_o [fm]	R_s [fm]	R_l [fm]	λ	δ_o	δ_s	δ_l
$[0.15, 0.25]$	1.30 ± 0.03	1.05 ± 0.03	1.92 ± 0.05	0.295 ± 0.004	0.0027 ± 0.0026	-0.1673 ± 0.0052	-0.2327 ± 0.0078
$[0.25, 0.35]$	1.21 ± 0.03	1.05 ± 0.03	1.67 ± 0.05	0.381 ± 0.005	0.0201 ± 0.0054	-0.1422 ± 0.0051	-0.2949 ± 0.0081
$[0.35, 0.45]$	1.10 ± 0.03	0.94 ± 0.03	1.37 ± 0.05	0.433 ± 0.007	0.0457 ± 0.0059	-0.0902 ± 0.0053	-0.2273 ± 0.0090
$[0.45, 0.60]$	0.93 ± 0.03	0.82 ± 0.03	1.17 ± 0.05	0.480 ± 0.009	0.0404 ± 0.0085	-0.0476 ± 0.0093	-0.1469 ± 0.0104

TABLE II: Fit results from a fit to data from $p+p$ collisions at $\sqrt{s}$= 200 GeV using Eq. 11 to parameterize the femtoscopic correlations and Eq. 13 for non-femtoscopic ones ("$\delta - q$ fit").

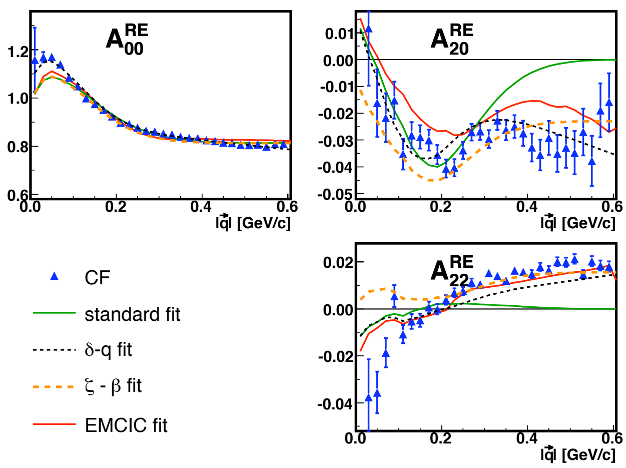

FIG. 3: (Color online) As for Fig. 2, but for $k_T = [0.25, 0.35]$ GeV/c.

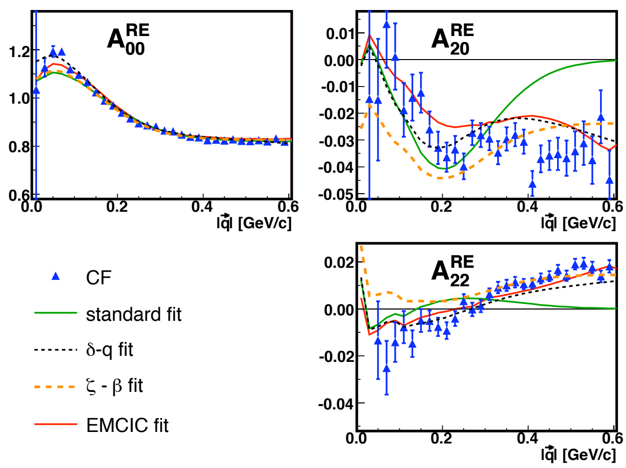

FIG. 4: (Color online) As for Fig. 2, but for $k_T = [0.35, 0.45]$ GeV/c.

than invent yet another ad-hoc functional form to better fit the data, we will consider the radii produced by all of these forms.

The fit parameters for these four fits, for each of the four k_T bins, are given in Tables I-IV. Considering first the non-femtoscopic correlations, we observe that the ad-hoc fit parameters $\delta_{O,S,L}$ and ζ and β in Tables III and II are different for each k_T bin. Due to their physical meaning, the EMCIC parameters M_{1-4} are fixed for all k_T values, as indicated in Table IV. Setting the characteristic particle mass to that of the pion and using Equations 16, 18 and 19, the non-femtoscopic parameters listed in Table IV correspond to the following values characteristic of the emitting system:

$$
\begin{aligned}
N &= 14.3 \pm 4.7 \\
\langle p_T^2 \rangle &= 0.17 \pm 0.06 \ (\mathrm{GeV/c})^2 \\
\langle p_z^2 \rangle &= 0.32 \pm 0.13 \ (\mathrm{GeV/c})^2 \\
\langle E^2 \rangle &= 0.51 \pm 0.11 \ \mathrm{GeV}^2 \\
\langle E \rangle &= 0.68 \pm 0.08 \ \mathrm{GeV}.
\end{aligned}
$$

These values are rather reasonable [44].

HBT radii from the different fits are plotted as a function of transverse mass in Figure 6. The treatment of the non-femtoscopic correlations significantly affects the magnitude of the femtoscopic length scales extracted from the fit, especially in the "out" and "long" directions, for which variations up to 50% in magnitude are observed. The dependence of the radii on $m_T \equiv \sqrt{k_T^2 + m^2}$ is quite similar in all cases. We discuss this dependence further in Section V.

k_T [GeV/c]	R_o [fm]	R_s [fm]	R_l [fm]	λ	ζ	β
$[0.15, 0.25]$	1.24 ± 0.04	0.92 ± 0.03	1.71 ± 0.04	0.392 ± 0.008	0.0169 ± 0.0021	-0.0113 ± 0.0019
$[0.25, 0.35]$	1.14 ± 0.05	0.89 ± 0.04	1.37 ± 0.08	0.378 ± 0.006	0.0193 ± 0.0034	-0.0284 ± 0.0031
$[0.35, 0.45]$	1.02 ± 0.04	0.81 ± 0.05	1.20 ± 0.07	0.434 ± 0.008	0.0178 ± 0.0029	-0.0289 ± 0.0032
$[0.45, 0.60]$	0.89 ± 0.04	0.71 ± 0.05	1.09 ± 0.06	0.492 ± 0.009	0.0114 ± 0.0023	-0.0301 ± 0.0041

TABLE III: Fit results from a fit to data from $p+p$ collisions at $\sqrt{s}$= 200 GeV using Eq. 11 to parameterize the femtoscopic correlations and Eq. 14 for non-femtoscopic ones ("$\zeta - \beta$ fit").

k_T [GeV/c]	R_o [fm]	R_s [fm]	R_l [fm]	λ	M_1 (GeV/c)$^{-2}$	M_2 (GeV/c)$^{-2}$	M_3 GeV^{-2}	M_4 GeV^{-1}
$[0.15, 0.25]$	1.06 ± 0.03	1.00 ± 0.04	1.38 ± 0.05	0.665 ± 0.000	0.43 ± 0.07	0.22 ± 0.06	1.51 ± 0.12	1.02 ± 0.09
$[0.25, 0.35]$	0.96 ± 0.02	0.95 ± 0.03	1.21 ± 0.03	0.588 ± 0.006				
$[0.35, 0.45]$	0.89 ± 0.02	0.88 ± 0.02	1.08 ± 0.04	0.579 ± 0.009				
$[0.45, 0.60]$	0.78 ± 0.04	0.79 ± 0.02	0.94 ± 0.03	0.671 ± 0.028				

TABLE IV: Fit results from a fit to data from $p+p$ collisions at $\sqrt{s}$= 200 GeV using Eq. 11 to parameterize the femtoscopic correlations and Eq. 15 for non-femtoscopic ones ("EMCIC fit").

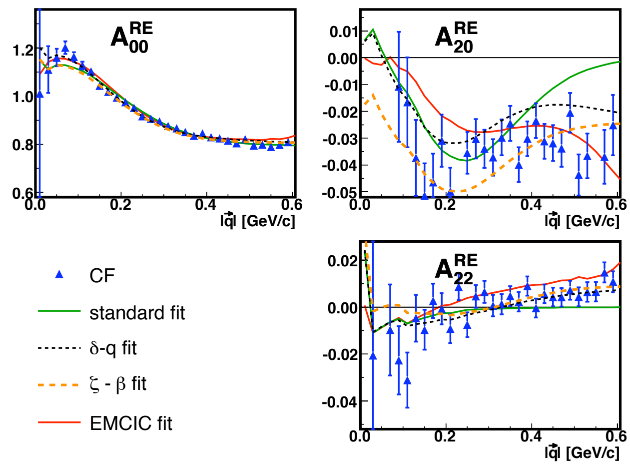

FIG. 5: (Color online) As for Fig. 2, but for $k_T = [0.45, 0.60]$ GeV/c.

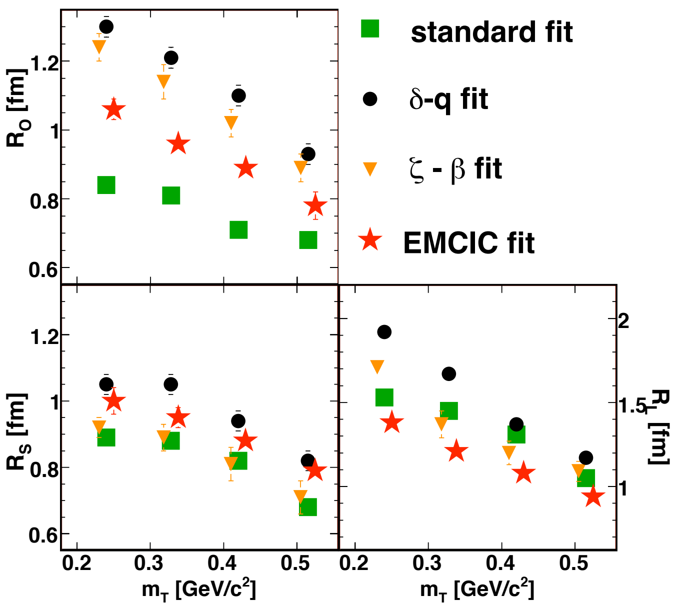

FIG. 6: (Color online) The m_T-dependence of the 3D femtoscopic radii in $p+p$ collisions at $\sqrt{s}$=200 GeV for different parameterizations of the non-femtoscopic correlations. See text for more details. Data have been shifted slightly in the abscissa, for clarity.

B. Transverse mass and multiplicity dependence of 1D femtoscopic radii

Since three-dimensional correlation functions encode more information about the homogeneity region than do one-dimensional correlation functions, they are also more statistics hungry. So most of the previous particle physics experiments have constructed and analyzed the latter. For the sake of making the connection between our results and existing world systematics, we perform similar analyses as those found in the literature.

The first important connection to make is for the m_T-dependence of HBT radii from minimum-bias $p+p$ collisions. We extract the one-dimensional HBT radius R_{inv} associated with the femtoscopic form in Equation 10, using three forms for the non-femtoscopic terms. For four selections in k_T, table V lists the fit parameters for the "standard" fit that neglects non-femtoscopic correlations altogether ($\Omega = 1$). Tables VI and VII list results when using the 1-dimensional $\delta - q$ form (Equation 12) and the EMCIC form (Equation 15), respectively. In performing the EMCICs fit, the non-femtoscopic parameters M_{1-4} were kept fixed at the values listed in Table IV.

The one-dimensional radii from the three different treatments of non-femtoscopic effects are plotted as a function of m_T in Figure 7. The magnitude of the radius using the ad-hoc $\delta - q$ fit is $\sim 25\%$ larger than that from either the standard or EMCIC fit, but again all show similar dependence on m_T.

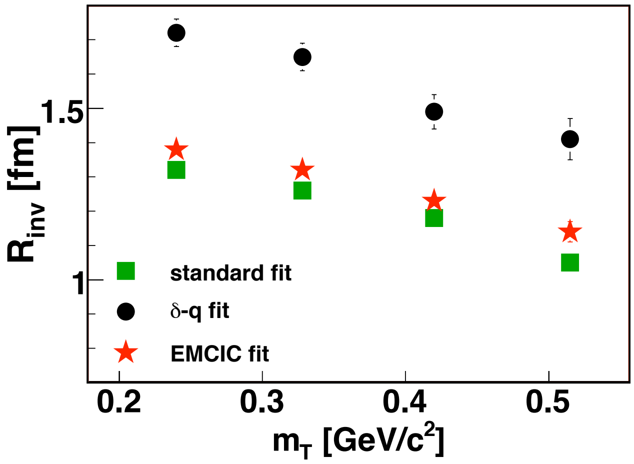

FIG. 7: (Color online) The m_T-dependence of R_{inv} from $p+p$ collisions at $\sqrt{s}$=200 GeV for different parameterizations of the non-femtoscopic correlations used in the fit procedure. See text for more details.

k_T [GeV/c]	R_{inv} [fm]	λ
[0.15,0.25]	1.32 ± 0.02	0.345 ± 0.005
[0.25,0.35]	1.26 ± 0.02	0.357 ± 0.007
[0.35,0.45]	1.18 ± 0.02	0.348 ± 0.008
[0.45,0.60]	1.05 ± 0.03	0.413 ± 0.012

TABLE V: Fit results from a fit to 1D correlation function from $p+p$ collisions at $\sqrt{s}$= 200 GeV using Eq. 6 to parameterize the femtoscopic correlations ("standard fit").

In order to compare with the multiplicity dependence of k_T-integrated HBT radii reported in high energy particle collisions, we combine k_T bins and separately analyze low ($dN_{ch}/d\eta \leq 6$) and high ($dN_{ch}/d\eta \geq 7$) multiplicity events. Fit parameters for common fitting functions are given in Table VIII, for minimum-bias and multiplicity-selected collisions.

Figure 8 shows the multiplicity dependence of the common one-dimensional HBT radius $R_{\rm inv}$,extracted by parameterizing the femtoscopic correlations according to Equation 10. Non-femtoscopic effects were either ignored ("standard fit" $\Omega=1$) or parameterized with the "$\delta-q$" (Eq. 12) or EMCIC (Eq. 15) functional form. In order to keep the parameter count down, the EMCIC, the kinematic parameters ($\langle p_T^2\rangle$, $\langle p_z^2\rangle$, $\langle E^2\rangle$, $\langle E\rangle$) were kept fixed to the values obtained from the 3-dimensional fit, and only N was allowed to vary. In all cases, $R_{\rm inv}$ is observed to increase with multiplicity. Parameterizing non-femtoscopic effects according to the EMCIC form gives similar results as a "standard" fit ignoring them, whereas the "$\delta-q$" form generates a ~ 0.3-fm offset, similar to all three- and one-dimensional fits discussed above.

k_T [GeV/c]	R_{inv} [fm]	λ	δQ_{inv}
[0.15,0.25]	1.72 ± 0.04	0.285 ± 0.007	0.237 ± 0.007
[0.25,0.35]	1.65 ± 0.04	0.339 ± 0.009	0.163 ± 0.008
[0.35,0.45]	1.49 ± 0.05	0.308 ± 0.011	0.180 ± 0.015
[0.45,0.60]	1.41 ± 0.06	0.338 ± 0.016	0.228 ± 0.017

TABLE VI: Fit results from a fit to 1D correlation function from $p+p$ collisions at $\sqrt{s}$= 200 GeV using Eq. 6 to parameterize the femtoscopic correlations and Eq. 12 for non-femtoscopic ones ("$\delta-q$ fit").

k_T [GeV/c]	R_{inv} [fm]	λ
[0.15,0.25]	1.38 ± 0.03	0.347 ± 0.005
[0.25,0.35]	1.32 ± 0.03	0.354 ± 0.006
[0.35,0.45]	1.23 ± 0.04	0.349 ± 0.009
[0.45,0.60]	1.14 ± 0.05	0.411 ± 0.013

TABLE VII: Fit results from a fit to 1D correlation function from $p+p$ collisions at $\sqrt{s}$= 200 GeV using Eq. 6 to parameterize the femtoscopic correlations and Eq. 15 for non-femtoscopic ones ("EMCICs fit"). The non-femtoscopic parameters M_{1-4} were not varied, but kept fixed to the values in Table IV.

Figure 9 shows results using Eq. 7 and Eq. 8. As discussed in Sec. IV A, the radius obtained from the latter formula is expected to be approximately twice as large as that from the former; hence we divided the first radius by a factor of 2 for comparison. These values will be compared with previously measured data in the next section.

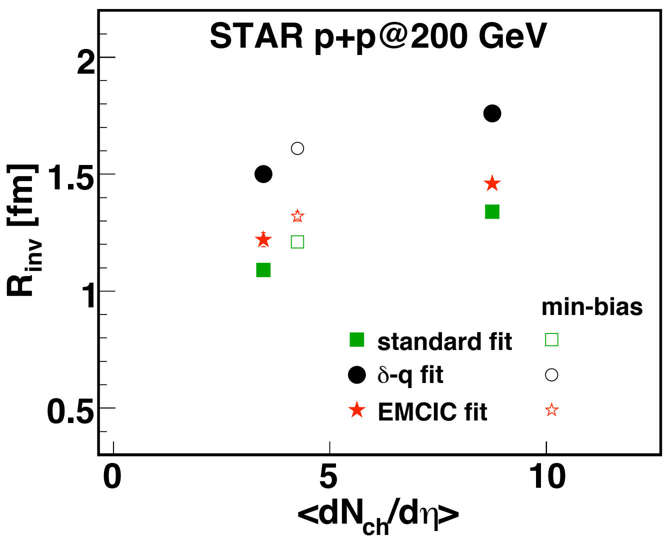

FIG. 8: (Color online) The multiplicity dependence of R_{inv} from $p+p$ collisions at $\sqrt{s}$=200 GeV for different parameterizations of the non-femtoscopic correlations. The particles within the range of $k_T=[0.15,0.60]$ GeV/c were used in the analysis.

V. COMPARISON WITH WORLD SYSTEMATICS

In this section, we make the connection between femtoscopic measurements in heavy ion collisions and those in par-

method	fit parameter	$\langle dN_{ch}/d\eta\rangle$		
		4.25 (min-bias)	3.47	8.75
standard fit	R_{inv}	1.21 ± 0.01	1.09 ± 0.02	1.34 ± 0.02
	λ	0.353 ± 0.003	0.347 ± 0.04	0.356 ± 0.03
$\delta-q$ fit	R_{inv}	1.61 ± 0.01	1.50 ± 0.03	1.76 ± 0.03
	λ	0.312 ± 0.003	0.275 ± 0.005	0.322 ± 0.007
	δQ_{inv}	-0.191 ± 0.003	-0.242 ± 0.005	-0.194 ± 0.006
EMCIC fit	R_{inv}	1.32 ± 0.02	1.22 ± 0.03	1.46 ± 0.02
	λ	0.481 ± 0.003	0.485 ± 0.003	0.504 ± 0.004
	N	14.3 ± 4.7	11.8 ± 7.1	26.3 ± 8.4
Eq. 7	R_G	1.00 ± 0.01	0.91 ± 0.01	1.07 ± 0.01
	λ	0.407 ± 0.004	0.390 ± 0.004	0.370 ± 0.006
Eq. 8	R_B	1.83 ± 0.01	1.69 ± 0.01	1.93 ± 0.01
	λ	0.364 ± 0.003	0.352 ± 0.004	0.332 ± 0.004

TABLE VIII: Multiplicity dependence of fit results to 1D correlation function from $p+p$ collisions at $\sqrt{s}$= 200 GeV for different fit parameterizations.

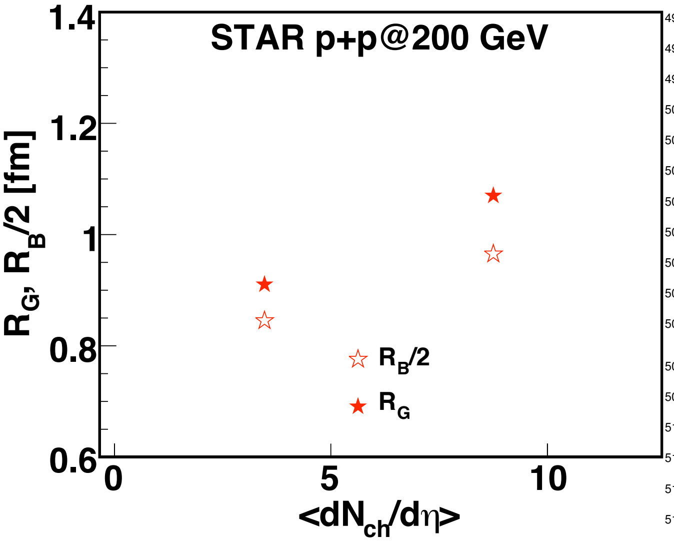

FIG. 9: (Color online) The multiplicity dependence of R_G and R_B from $p+p$ collisions at $\sqrt{s}$=200 GeV. The particles within the range of $k_T = [0.15, 0.60]$ GeV/c were used in the analysis.

ticle physics, by placing our results in the context of world systematics from each.

A. Results in the Context of Heavy Ion Systematics

The present measurement represents the first opportunity to study femtoscopic correlations from hadronic collisions and heavy ion collisions, using the same detector, reconstruction, analysis and fitting techniques. The comparison should be direct, and differences in the extracted HBT radii should arise from differences in the source geometry itself. In fact, especially in recent years, the heavy ion community has generally arrived at a consensus among the different experiments, as far as analysis techniques, fitting functions and reference frames to use. This, together with good documentation of event selection and acceptance cuts, has led to a quantitatively consistent world systematics of femtoscopic measurements in heavy ion collisions over two orders of magnitude in collision energy [11]; indeed, at RHIC, the agreement in HBT radii from the different experiments is remarkably good. Thus, inasmuch as STAR's measurement of HBT radii from $p+p$ collisions may be directly compared with STAR's HBT radii from Au+Au collisions, they may be equally well compared to the world's systematics of all heavy ion collisions.

As with most heavy ion observables in the soft sector [51], the HBT radii R_s and R_l scale primarily with event multiplicity [11] (or, at lower energies, with the number of particles of different species [52, 53]) rather than energy or impact parameter. The radius R_o, which nontrivially combines space and time, shows a less clear scaling [11], retaining some energy dependence. As seen in Figure 10, the radii from $p+p$ collisions at $\sqrt{s}$=200 GeV fall naturally in line with this multiplicity scaling. On the scale relevant for this comparison, the specific treatment of non-femtoscopic correlations is unimportant.

One of the most important systematics in heavy ion femtoscopy is the m_T-dependence of HBT radii, which directly measures space-momentum correlations in the emitting source at freeze-out; in these large systems, the m_T-dependence is often attributed to collective flow [6]. As we saw in Figure 6, a significant dependence is seen also for $p+p$ collisions. Several authors [e.g. 18, 29, 30, 35, 54] have remarked on the qualitative "similarity" of the m_T-dependence of HBT radii measured in high energy particle collisions, but the first direct comparison is shown in Figure 11. There, the ratios of the three dimensional radii in Au+Au collisions to p+p radii obtained with different treatments of the non-femtoscopic correlations, are plotted versus m_T. Well beyond qualitative similarity, the ratios are remarkably flat– i.e. the m_T-dependence in $p+p$ collisions is quantitatively almost identical to that in Au+Au collisions at RHIC. We speculate on the possible meaning of this in Section V B.

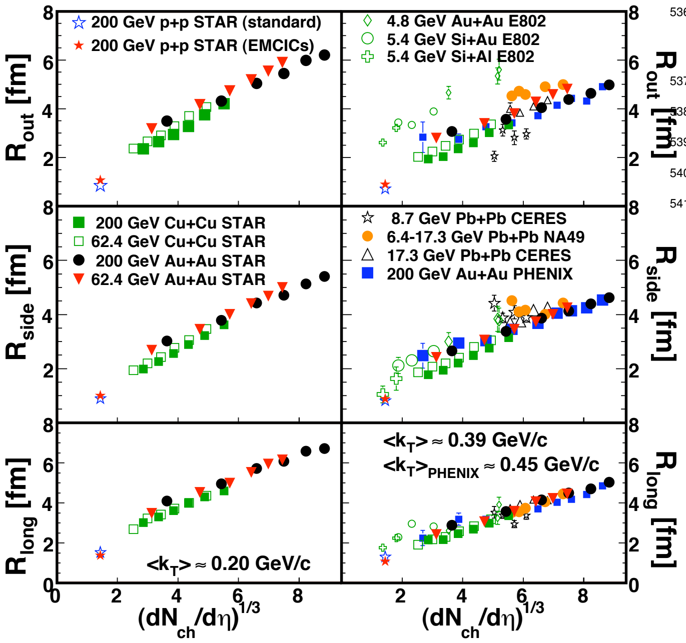

FIG. 10: (Color online) The multiplicity dependence of the HBT radii from $p+p$, $Cu+Cu$ [48] and $Au+Au$ [47, 48] collisions from STAR compared with results from other experiments [11]. Left and right panels show radii measured with $\langle k_T \rangle \approx 0.2$ and 0.39 GeV/c, respectively. Radii from $p+p$ collisions are shown by blue ("standard fit") and red ("EMCIC fit") stars.

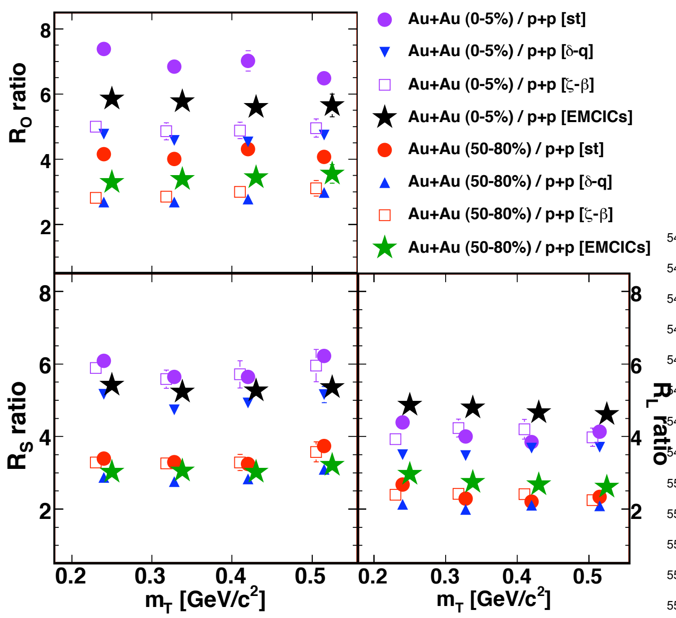

FIG. 11: (Color online) The ratio of the HBT radii from $Au+Au$ collisions [47] to results from $p+p$ collisions plotted versus the transverse mass.

B. Results in the context of high-energy particle measurements

Recently, a review of the femtoscopic results [20] from particle collisions like $p+p$, $p+\bar{p}$ and $e^{+}+e^{-}$ studied at different energies has been published. Here, we would like to compare STAR results from $p+p$ collisions at $\sqrt{s}$=200 GeV with world systematics.

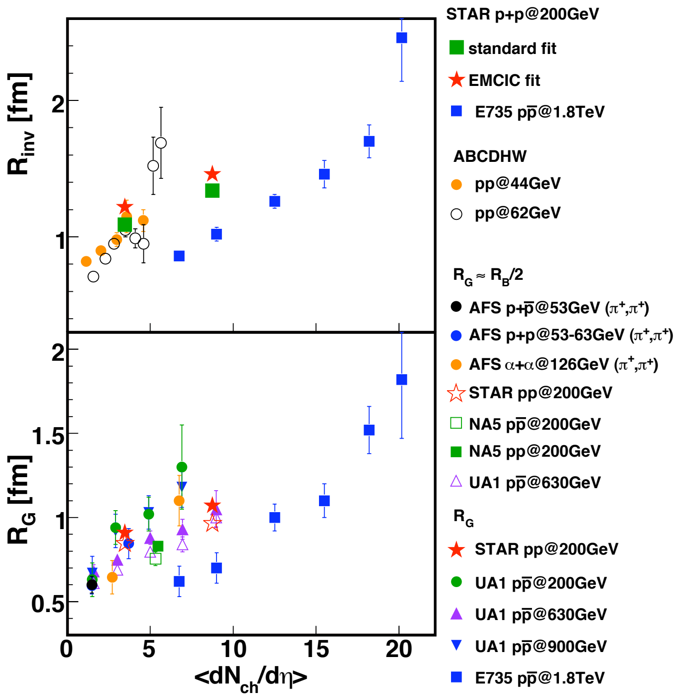

FIG. 12: (Color online) The multiplicity dependence of 1D femtoscopic radii from hadronic collisions measured by STAR, E735 [35], ABCDHW [55], UA1 [56], AFS [57] and NA5 [58].

Figure 12 shows STAR results plotted together with data collected in [20], as a function of multiplicity. The upper panel shows R_{inv} radius and the lower panel R_G or $R_B/2$. Radii from each experiment increase with multiplicity. However, in contrast to the "universal" scaling observed in heavy ion collisions (c.f. Figure 10), any such scaling is much more approximate, here.

There are several possible reasons for this [20]. Clearly one possibility is that there is no universal multiplicity dependence of the femtoscopic scales; the underlying physics driving the space-time freezeout geometry may be quite different, considering $\sqrt{s}$ varies from 44 to 1800 GeV in the plot. However, even if there were an underlying universality between these systems, it is not at all clear that it would appear in this figure, due to various difficulties in tabulating historical data [20]. Firstly, as discussed in Section II the experiments used different fitting functions to extract the HBT radii, making direct comparison between them difficult. Secondly, as we have shown, the radii depend on both multiplicity and k_T. Since, for statistical reasons, the results in Figure 10 are integrated over the acceptance of each experiment, and

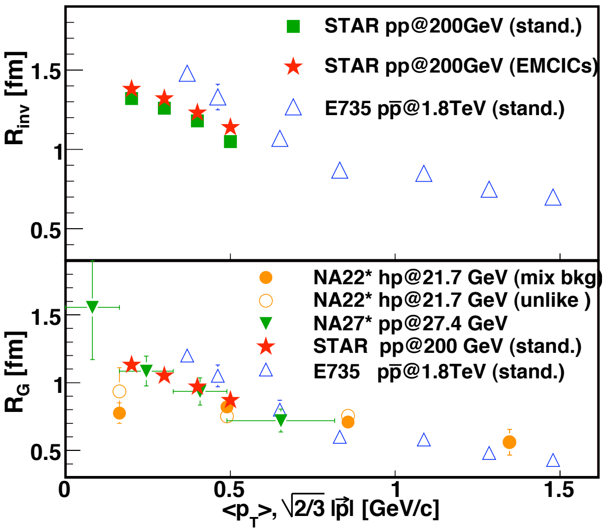

FIG. 13: (Color online) The transverse mass dependence of 1D femtoscopic radii from elementary particle collisions. Data from E735 [35], NA27 [40] and NA22 [29].

these acceptances differ strongly, any universal scaling would be obscured. For example, since the acceptance of Tevatron experiment E735 [35] is weighted towards higher k_T than the other measurements, one expects a systematically lower HBT radius, at a given multiplicity. Indeed, even the "universal" multiplicity scaling in heavy ion collisions is only universal for a fixed selection in k_T. Thirdly, these experiments did not follow a standard method of measuring and reporting multiplicity; thus the determination of $\langle dN\mathrm{ch}/d\eta\rangle$ for any given experiment shown in Figure 10 is only approximate.

From the discussion above, we cannot conclude definitively that there is– or is not– a universal multiplicity scaling of femtoscopic radii in high energy hadron-hadron collisions. We conclude only that an increase of these radii with multiplicity is observed in all measurements for which $\sqrt{s} \gtrsim 40$ GeV and that the present analysis of $p+p$ collisions is consistent with world systematics.

In Section IV, we discussed the p_T-dependence of HBT radii observed in our analysis. Previous experiments on high-energy collisions between hadrons– and even leptons– have reported similar trends. As discussed above, direct comparisons with historical high-energy measurements are problematic. Nevertheless, good qualitative and even semi-quantitative agreement between measurements of 1-dimensional HBT radii is observed Figure 13. Indeed, the consistency between the data is impressive, considering that the SPS [29, 40] collisions took place at an order of magnitude lower in $\sqrt{s}$, while the Tevatron data [35] was taken at an order of magnitude higher $\sqrt{s}$.

Systematics in 3-dimensional HBT radii from hadron collisions are less clear and less abundant, though our measurements are again qualitatively similar to those reported at the SPS, as shown in Figure 14. There, we also plot recent results from $e^+ - e^-$ collisions at LEP; in those 3-dimensional analyses, the "lonngitudinal" direction is the thrust axis, whereas the beam axis is used in hadron-hadron collisions, as in heavy ion collisions.

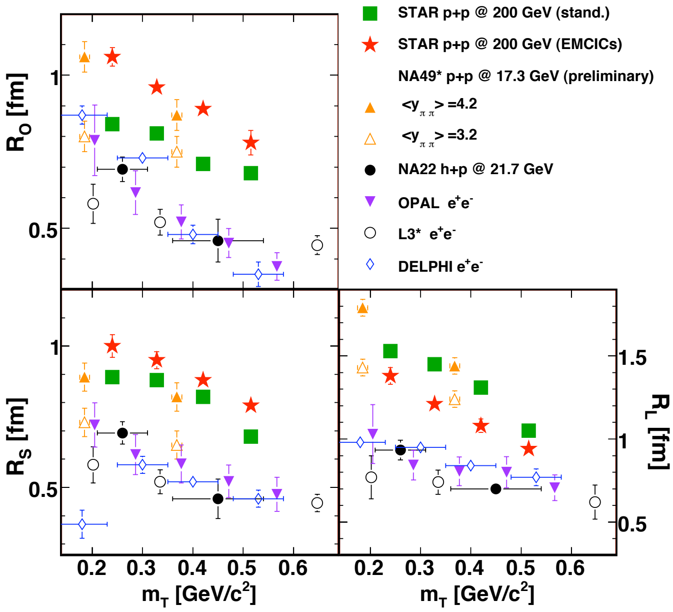

FIG. 14: (Color online) The transverse mass dependence of 3D femtoscopic radii from elementary particle collisions. Data from NA22 [29], NA49 preliminary [59], OPAL [30], L3 [39], DELPHI [60].

VI. DISCUSSION

We have seen that HBT radii from $p+p$ collisions at RHIC are qualitatively consistent with the trends observed in particle collisions over a variety of collision energies. Further, they fall quantitatively into the much better-defined world systematics for heavy ion collisions at RHIC and similar energies. Particularly intriguing is the nearly identical dependence on m_T of the HBT radii in $p+p$ and heavy ion collisions, as this dependence is supposed [23, 61] to reflect the underlying dynamics of the latter. Several possible sources of an m_T dependence of HBT radii in small systems have been put forward to explain previous measurements.

1. Alexander *et al.* [62, 63] have suggested that the Heisenberg uncertainty principle can produce the transverse momentum dependence of femtoscopic radii in $e^+ + e^-$ collisions. However, as discussed in [20], a more detailed study of the results from $e^+ + e^-$ collisions complicates the quantitative comparisons of the data from various experiments and thus the interpretation. Additionally, Alexander's explanation applies only to the longitudinal direction (R_l), so could not explain the dependence of all three radii.

2. In principle, string fragmentation should also generate space-momentum correlations in small systems, hence an m_T dependence of the HBT radii. However, there are almost no quantitative predictions that can be compared with

data. The numerical implementation PYTHIA, which incorporates the Lund string model into the soft sector dynamics, implements HBT only as a crude parameterization designed to mock up the effect [c.f. Section 12.4.3 of 64] for the purpose of estimating distortions to W-boson invariant mass spectrum. Any Bose-Einstein correlation function may be dialed into the model, with 13 parameters to set the HBT radius, lambda parameter, and correlation shape; there is no first-principles predictive power. On more general grounds, the mass dependence of the femtoscopic radii cannot be explained within a Lund string model [65–67].

3. Long-lived resonances may also generate the space-momentum dependence of femtoscopic radii [68]. However, as discussed in [20], the resonances would affect the HBT radii from $p+p$ collisions differently than those from $Au+Au$ collisions, since the scale of the resonance "halo" is fixed by resonannce lifetimes while the scale of the "core" is different for the two cases. Thus it would have to be a coincidence that the same m_T dependence is observed in both systems. Nevertheless, this avenue should be explored further.

4. Białas *et al.* have introduced a model [65] based on a direct proportionality between the four-momentum and space-time freeze-out position; this model successfully described data from $e^+ + e^-$ collisions. The physical scenario is based on freezeout of particles emitted from a common tube, after a fixed time of 1.5 fm/c. With a very similar model, Humanic [69] was unable to reproduce HBT radii measured at the Tevatron [35] without strong additional hadronic rescattering effects. With rescattering in the final state, both the multiplicity- and the m_T-dependence of the radii were reproduced [69].

5. It has been suggested [18, 29, 30, 35, 70] that the p_T-dependence of HBT radii in very small systems might reflect bulk collective flow, as it is believed to do in heavy ion collisions. This is the only explanation that would automatically account for the nearly identical p_T-scaling discussed in Section V A. However, it is widely believed that the system created in $p+p$ collisions is too small to generate bulk flow.

The remarkable similarity between the femtoscopic systematics in heavy ion and hadron collisions may well be coincidental. Given the importance of the m_T-dependence of HBT radii in heavy ion collisions, and the unclear origin of this dependence in hadron collisions, further theoretical investigation is clearly called for. Additional comparative studies of other soft-sector observables (e.g. spectra) may shed further light onto this coincidence.

VII. SUMMARY

We have presented a systematic femtoscopic analysis of two-pion correlation functions from p+p collisions at RHIC. In addition to femtoscopic effects, the data show correlations due to energy and momentum conservation. Such effects have been observed previously in low-multiplicity measurements at Tevatron, SPS, and elsewhere. In order to compare to historical data and to identify systematic effects on the HBT radii, we have treated these effects with a variety of empirical and physically-motivated formulations. While the overall magnitude of the geometric scales vary with the method, the important systematics do not.

In particular, we observe a significant positive correlation between the one- and three-dimensional radii and the multiplicity of the collision, while the radii decrease with increasing transverse momentum. Qualitatively, similar multiplicity and momentum systematics have been observed previously in measurements of hadron and electron collisions at the Sp$\bar{\text{p}}$S, Tevatron, ISR and LEP. However, the results from these experiments could not be directly compared to those from heavy ion collisions, due to differences in techniques, fitting methods, and acceptance.

Thus, the results presented here provide a unique possibility for a direct comparison of femtoscopy in p+p and A+A collisions. We have seen very similar p_T and multiplicity scaling of the femtoscopic scales in p+p as in A+A collisions, independent of the fitting method employed. Given the importance of femtoscopic systematics in understanding the bulk sector in $Au+Au$ collisions, further exploration of the physics behind the same scalings in $p+p$ collisions is clearly important, to understand our "reference" system. The similarities observed could indicate a deep connection of the underlying bulk physics driving systems much larger than– and on the order of– the confinement scale. At the Large Hadron Collider, similar comparisons will be possible, and the much higher energies available will render conservation law-driven effects less important.

[1] J. Adams et al. (STAR) (2005), nucl-ex/0501009.
[2] K. Adcox et al. (PHENIX) (2004), nucl-ex/0410003.
[3] B. B. Back et al. (2004), nucl-ex/0410022.
[4] I. Arsene et al. (BRAHMS) (2004), nucl-ex/0410020.
[5] E. Schnedermann, J. Sollfrank, and U. W. Heinz, Phys. Rev. **C48**, 2462 (1993), nucl-th/9307020.
[6] F. Retiere and M. A. Lisa, Phys. Rev. **C70**, 044907 (2004), nucl-th/0312024.
[7] J.-Y. Ollitrault, Phys. Rev. **D46**, 229 (1992).
[8] S. A. Voloshin, A. M. Poskanzer, and R. Snellings (2008), 0809.2949.
[9] P. F. Kolb and U. Heinz (2003), nucl-th/0305084.
[10] R. Lednicky, Nucl. Phys. **A774**, 189 (2006), nucl-th/0510020.
[11] M. A. Lisa, S. Pratt, R. Soltz, and U. Wiedemann, Ann. Rev. Nucl. Part. Sci. **55**, 357 (2005), nucl-ex/0505014.
[12] S. V. Akkelin and Y. M. Sinyukov, Phys. Lett. **B356**, 525 (1995).
[13] R. Lednicky, V. L. Lyuboshits, B. Erazmus, and D. Nouais, Phys. Lett. **B373**, 30 (1996).
[14] U. W. Heinz and P. F. Kolb (2002), hep-ph/0204061, URL `http://arXiv.org/pdf/hep-ph/0204061`.
[15] S. Pratt, Phys. Rev. **D33**, 1314 (1986).

[16] D. H. Rischke and M. Gyulassy, Nucl. Phys. **A608**, 479 (1996), nucl-th/9606039.

[17] S. Bekele et al. (2007), 0706.0537.

[18] W. Kittel, Acta Phys. Polon. **B32**, 3927 (2001), hep-ph/0110088.

[19] G. Alexander, Rept. Prog. Phys. **66**, 481 (2003), hep-ph/0302130.

[20] Z. Chajecki, Acta Phys. Polon. **B40**, 1119 (2009), 0901.4078.

[21] G. I. Kopylov, Phys. Lett. **B50**, 472 (1974).

[22] P. Jacobs and X.-N. Wang, Prog. Part. Nucl. Phys. **54**, 443 (2005), hep-ph/0405125.

[23] S. Pratt, Phys. Rev. Lett. **53**, 1219 (1984).

[24] G. Bertsch, M. Gong, and M. Tohyama, Phys. Rev. **C37**, 1896 (1988).

[25] P. Danielewicz and S. Pratt (2005), nucl-th/0501003.

[26] P. Danielewicz and S. Pratt, Phys. Rev. **C75**, 034907 (2007), nucl-th/0612076.

[27] Z. Chajecki and M. Lisa, Phys. Rev. **C78**, 064903 (2008), 0803.0022.

[28] P. Avery et al. (CLEO), Phys. Rev. **D32**, 2294 (1985).

[29] N. M. Agababyan et al. (EHS/NA22), Z. Phys. **C71**, 405 (1996).

[30] G. Abbiendi et al. (OPAL), Eur. Phys. J. **C52**, 787 (2007), 0708.1122.

[31] J. L. Bailly et al. (NA23), Z. Phys. **C43**, 341 (1989).

[32] J. Uribe et al. (BNL-E766), Phys. Rev. **D49**, 4373 (1994).

[33] G. I. Kopylov and M. I. Podgoretsky, Sov. J. Nucl. Phys. **15**, 219 (1972).

[34] D. H. Boal, C. K. Gelbke, and B. K. Jennings, Rev. Mod. Phys. **62**, 553 (1990).

[35] T. Alexopoulos et al., Phys. Rev. **D48**, 1931 (1993).

[36] M. G. Bowler, Phys. Lett. **B270**, 69 (1991).

[37] Y. Sinyukov, R. Lednicky, S. V. Akkelin, J. Pluta, and B. Erazmus, Phys. Lett. **B432**, 248 (1998).

[38] D. Buskulic et al. (ALEPH), Z. Phys. **C64**, 361 (1994).

[39] P. Achard et al. (L3), Phys. Lett. **B524**, 55 (2002), hep-ex/0109036.

[40] M. Aguilar-Benitez et al. (LEBC-EHS), Z. Phys. **C54**, 21 (1992).

[41] P. Abreu et al. (DELPHI), Z. Phys. **C63**, 17 (1994).

[42] P. Abreu et al. (DELPHI), Phys. Lett. **B286**, 201 (1992).

[43] Z. Chajecki, AIP Conf. Proc. **828**, 566 (2006), nucl-ex/0511035.

[44] Z. Chajecki and M. Lisa, Phys. Rev. **C79**, 034908 (2009), 0807.3569.

[45] C. Adler et al. (STAR), Phys. Rev. Lett. **87**, 082301 (2001), nucl-ex/0107008.

[46] J. Adams et al. (STAR), Phys. Rev. Lett. **93**, 012301 (2004), nucl-ex/0312009.

[47] J. Adams et al. (STAR), Phys. Rev. **C71**, 044906 (2005), nucl-ex/0411036.

[48] B. I. Abelev et al. (STAR) (2009), 0903.1296.

[49] M. Anderson et al., Nucl. Instrum. Meth. **A499**, 659 (2003), nucl-ex/0301015.

[50] A. Kisiel and D. A. Brown (2009), 0901.3527.

[51] H. Caines, Eur. Phys. J. **C49**, 297 (2007), nucl-ex/0609004.

[52] D. Adamova et al. (CERES), Phys. Rev. Lett. **90**, 022301 (2003), nucl-ex/0207008.

[53] M. A. Lisa and S. Pratt (2008), 0811.1352.

[54] T. Alexopoulos et al., Phys. Lett. **B528**, 43 (2002), hep-ex/0201030.

[55] A. Breakstone et al. (Ames-Bologna-CERN-Dortmund-Heidelberg-Warsaw), Z. Phys. **C33**, 333 (1987).

[56] C. Albajar et al. (UA1), Phys. Lett. **B226**, 410 (1989).

[57] T. Akesson et al. (Axial Field Spectrometer), Phys. Lett. **B129**, 269 (1983).

[58] C. De Marzo et al., Phys. Rev. **D29**, 363 (1984).

[59] R. Ganz (NA49), Nucl. Phys. **A661**, 448 (1999), nucl-ex/9909003.

[60] A. Smirnova (1999), *Soft Multihadron Dynamics*, Hackensack, USA: World Scientific (1999) eds. N.G. Antoniou et al., pp.157-167.

[61] U. W. Heinz and B. V. Jacak, Ann. Rev. Nucl. Part. Sci. **49**, 529 (1999), nucl-th/9902020.

[62] G. Alexander, I. Cohen, and E. Levin, Phys. Lett. **B452**, 159 (1999), hep-ph/9901341.

[63] G. Alexander, Phys. Lett. **B506**, 45 (2001), hep-ph/0101319.

[64] T. Sjostrand, S. Mrenna, and P. Skands, JHEP **05**, 026 (2006), hep-ph/0603175.

[65] A. Bialas, M. Kucharczyk, H. Palka, and K. Zalewski, Phys. Rev. **D62**, 114007 (2000), hep-ph/0006290.

[66] G. Alexander (2001), hep-ph/0108194.

[67] G. Alexander, Acta Phys. Polon. **B35**, 69 (2004), hep-ph/0311114.

[68] U. A. Wiedemann and U. W. Heinz, Phys. Rev. **C56**, 3265 (1997), nucl-th/9611031.

[69] T. J. Humanic, Phys. Rev. **C76**, 025205 (2007), nucl-th/0612098.

[70] T. Csorgo, M. Csanad, B. Lorstad, and A. Ster, Acta Phys. Hung. **A24**, 139 (2005), hep-ph/0406042.